



Synthesis and enhanced photocatalytic activity of g-C₃N₄ hybridized CdS nanoparticles

QING YING LIU¹, YI LING QI¹, YI FAN ZHENG² and XU CHUN SONG^{1,*}

¹Department of Chemistry, Fujian Normal University, Fuzhou 350007, People's Republic of China

²Research Center of Analysis and Measurement, Zhejiang University of Technology, Hangzhou 310014, People's Republic of China

*Author for correspondence (songxuchunfj@163.com)

MS received 4 August 2016; accepted 7 May 2017; published online 6 December 2017

Abstract. The highly effective g-C₃N₄ hybridized CdS photocatalysts were synthesized via a successive calcination and hydrothermal process. The as-prepared photocatalysts were characterized by X-ray powder diffraction, transmission electron microscopy and UV–Vis diffuse reflectance spectroscopy. The photocatalytic performance of the C₃N₄/CdS nanocomposites was evaluated by the photodegradation of RhB under visible light irradiation. The results showed that photocatalytic ability of the C₃N₄/CdS nanocomposites was higher than that of pure C₃N₄ and CdS. The enhanced photocatalytic activity could be attributed to the high separation efficiency of the photo-excited electron-hole pairs. A possible mechanism of the photocatalytic degradation of RhB on C₃N₄/CdS nanocomposites was also proposed.

Keywords. C₃N₄; CdS; photocatalytic; nanocomposites.

1. Introduction

Artificial semiconductor photocatalysis offers a viable strategy for removal of water pollutants because it represents an easy method to utilize the energy of either artificial illumination or natural sunlight [1–4]. Recently, it has been confirmed that materials with conjugative π structure (graphene-like carbon and C₆₀, etc.) have high photocatalytic performance, which has attracted an extensive interest in photocatalytic applications [5]. Graphite-like C₃N₄ exhibits high photocatalytic activity for degradation of organic pollution under visible light irradiation due to its unique optical properties, suitable band gap, high chemical and thermal stability [6,7]. Moreover, a lot of results concerning the g-C₃N₄ hybridization have also been reported as effective ways to enhance the catalytic properties of photocatalysts. For instance, Wang *et al* [8] synthesized C₃N₄/Bi₂WO₆ photocatalyst, which showed higher photocatalytic activity than that of pure Bi₂WO₆ or C₃N₄ and the enhanced photocatalytic activity could be attributed to the rapid photo-induced charge separation. A novel BiOBr–C₃N₄ heterojunctions have also been fabricated by depositing BiOBr onto the surface of g-C₃N₄ and showed preferable photocatalytic activity on RhB decomposition under visible or indoor light [9]. AgX@g-C₃N₄ (X = Cl, Br and I) photocatalysts were recently reported showing excellent visible light-driven photocatalytic activity due to their higher photostability and the efficient separation of photogenerated charge carrier [10]. Although the hybrid C₃N₄ photocatalysts displayed excellent photocatalytic performance, they did not meet all the needs in

practical applications, such as highly efficient decomposition of organic contaminants and the effective utilization of visible light. Therefore, the development of a highly effective visible-light active photocatalyst is still desired.

CdS is an attractive visible-light photocatalyst because of its desired band-gap width (2.4 eV) and oxidation and reduction potentials [11]. However, the photocatalytic efficiency of nano-CdS is severely restricted by photocorrosion under strong illumination and higher recombination rates of photoexcited charge carriers [12]. CdS may also act as important sensitizers, which can sensitize the wide band gap semiconductor and thus improve the photocatalytic activity and stability of the photocatalyst. For example, ZnO/CdS core/shell nanorods were synthesized by a surface-functionalized method and displayed higher photocatalytic activity for the degradation of RhB under simulated solar radiation [13]. Similarly, the CdS/WO₃ nanojunction artificial photosynthesis system is successfully constructed, and the rate of H₂ evolution on the photocatalysts is five times as high as that of pure CdS [14]. Recently, Huang and others [15] have successfully fabricated the CdS/g-C₃N₄ core/shell configuration with high photo-catalytic activity and excellent photostability, which is a very promising candidate for possible practical application. Therefore, it is highly desired that the combination of CdS and C₃N₄ may be an ideal system to increase the separation efficiency of photogenerated electron-hole pairs and at the same time extend the absorption to visible light. In this work, we reported the synthesis of the C₃N₄/CdS nanocomposites through a calcinations–hydrothermal route, which exhibited extended absorption of visible light and

enhanced photodegradation efficiency of RhB. Compared with pure C_3N_4 and CdS, C_3N_4/CdS nanocomposites showed a higher photocatalytic activity due to efficient separation of photo-induced electron-hole pairs. The possible mechanism of the enhanced visible light photocatalytic activity of C_3N_4/CdS nanocomposites is also discussed in detail.

2. Experimental

2.1 Preparation of C_3N_4/CdS nanocomposites

The C_3N_4 powder was prepared by a facile thermal polycondensation of melamine in air. Typically, 5 g of melamine powder was put into a crucible and then heated to 520°C in a muffle furnace with a rate of $10^\circ\text{C min}^{-1}$ for 4 h. The C_3N_4/CdS nanocomposites were prepared by a hydrothermal method. In a typical procedure, appropriate amount of C_3N_4 powder was initially added into 20 ml of 0.25 M $\text{CdCl}_2 \cdot 2.5\text{H}_2\text{O}$ aqueous solution and ultrasonicated for 10 min. Subsequently, 20 ml of 0.25 M $\text{Na}_2\text{S} \cdot 9\text{H}_2\text{O}$ aqueous solution was added into the above solution and stirred for 30 min. Then, the mixture was transferred into a Teflon-lined stainless-steel autoclave with a capacity of 50 ml, which was heated at 180°C for 12 h. Later the product was collected by centrifugation, washed with deionized water and then dried at 80°C for 6 h. For comparison, different mass ratios of C_3N_4/CdS at 5, 10 and 15% were synthesized with the same procedure and denoted as 5% C_3N_4/CdS , 10% C_3N_4/CdS and 15% C_3N_4/CdS , respectively.

2.2 Characterization

X-ray powder diffraction (XRD) of the as-prepared photocatalysts was investigated on a Thermo ARL SCINTAG X'TRA X-ray diffractometer using $\text{Cu-K}\alpha$ radiation ($\lambda = 0.154056 \text{ nm}$). High-resolution transmission electron microscopy (HRTEM, Tecnai G2 F30 S-Twin) was employed to observe the morphology and microstructures of as-prepared samples. The optical absorption properties of the samples were investigated via UV-Vis diffuse reflectance spectroscopy (DRS) using a Hitachi U-3010 spectrometer.

2.3 Photocatalytic experiments

The photocatalytic activities of the obtained C_3N_4/CdS nanocomposites were evaluated by degrading RhB under visible light. Visible irradiation was obtained from a 300 W Xenon lamp (CEL-HXF300) with a 420 nm cut-off filter. In each experiment, 50 mg of photocatalyst was transferred into 100 ml of RhB ($C_0 = 1 \times 10^{-5} \text{ M}$) with constant stirring. The above suspension was stirred in the dark before irradiation in order to reach the adsorption equilibrium between RhB and the catalyst. At each interval, 5 ml of the suspension was withdrawn and centrifuged to remove the photocatalyst. The concentration of RhB was analysed by recording

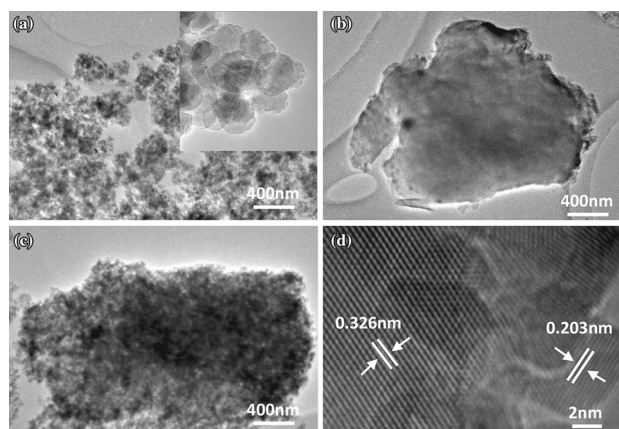


Figure 1. TEM images of (a) CdS, (b) C_3N_4 , (c) 10% C_3N_4/CdS and (d) HRTEM image of the 10% C_3N_4/CdS .

the absorbance at the characteristic band of 553 nm using a UV759S UV-Vis spectrophotometer.

3. Results and discussions

Transmission electron microscopy (TEM) and HRTEM images were taken to analyse the morphology and microstructure of the samples. Figure 1a shows the TEM image of pure CdS. Nanoparticles structure with an average particle size of about 15 nm can be observed on the image suggesting the nanoparticle morphology of CdS. However, pure C_3N_4 (figure 1b) shows quite different morphology with 2D lamellar structure and smooth surfaces. Moreover, it can be clearly investigated from the TEM image of 10% C_3N_4/CdS nanocomposite (figure 1c) that the CdS nanoparticles were deposited on the surface of C_3N_4 nanosheets. The HRTEM image of the 10% C_3N_4/CdS nanocomposite is shown in figure 1d. The lattice plane separation of 0.326 nm can be assigned to the (002) crystal plane of C_3N_4 . Furthermore, the measured lattice spacing of 0.203 nm corresponds to the (110) plane of CdS. These results may suggest the formation of nanocomposites between C_3N_4 and CdS.

XRD patterns of CdS, C_3N_4 and 10% C_3N_4/CdS are shown in figure 2. It can be observed that the pure CdS is crystallized in a hexagonal Wurtzite structure with lattice parameters $a = 4.131 \text{ \AA}$ and $c = 6.735 \text{ \AA}$ (JCPDS no. 41-1049). The C_3N_4 sample exhibits two pronounced peaks at 27.4 and 13.1° , which corresponds to the (002) and (100) diffraction planes of the graphite-like C_3N_4 [16]. The XRD pattern of the 10% C_3N_4/CdS nanocomposites is similar to that of the pure CdS. No characteristic peak of C_3N_4 was examined in the C_3N_4/CdS nanocomposites, which might be ascribed to the low C_3N_4 amount and its relative weaker crystallinity.

The UV-Vis diffuse reflectance spectra of pure CdS, C_3N_4 and 10% C_3N_4/CdS are shown in figure 3a. It can be seen that the pure C_3N_4 and CdS both have absorbance in the

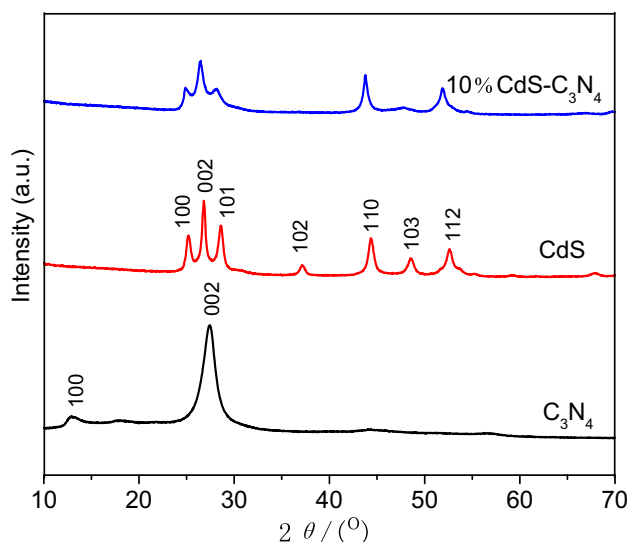


Figure 2. XRD patterns of (a) CdS, (b) C_3N_4 and (c) 10% C_3N_4/CdS .

visible-light range with the onset absorption of C_3N_4 about 460 nm and absorption edge of CdS around 570 nm. The absorbance of 10% C_3N_4/CdS is also in the visible-light region with a mixed absorption property of CdS and C_3N_4 and an obvious decrease of the absorption intensity. The band gaps of C_3N_4 and CdS can be calculated by the equation $A(h\nu - E_g)^{n/2} = \alpha h\nu$ [17], where A , h , ν , E_g and α are constants, the Planck's constant, the light frequency, the band-gap energy and absorption coefficient, respectively. The value of the exponent n is determined by the type of optical transition of the sample and is defined to be 4 for an indirect transition. The band-gap energy (E_g) of C_3N_4 and CdS can be estimated from a plot of $(\alpha h\nu)^{1/2}$ vs. energy ($h\nu$). Thus, the E_g of the C_3N_4 and CdS are determined to be 2.62 and 2.02 eV, respectively (figure 3b). The conduction band potentials (E_{CB}) of a semiconductor can be calculated by the following empirical equation $E_{CB} = X - E_c - 0.5E_g$ [18], where X is the absolute electronegativity of the semiconductor, E_c is the energy of free electrons on the hydrogen scale (about 4.5 eV), and the valence band (E_{VB}) can be obtained by $E_{VB} = E_{CB} + E_g$. The X values for C_3N_4 and CdS are 4.73 and 5.19 eV; thus the E_{CB} values of C_3N_4 and CdS are calculated to be -1.08 and -0.32 eV, and the E_{VB} value of C_3N_4 and CdS are estimated to be 1.54 and 1.70 eV, respectively.

The photocatalytic activities of pure CdS, C_3N_4 and C_3N_4/CdS nanocomposites were evaluated using RhB as a target pollutant under visible light irradiation. As shown in figure 4, the photodegradation of RhB over CdS and C_3N_4 was about 60.9 and 47.4%, respectively, and all C_3N_4/CdS nanocomposites showed higher photocatalytic activity than pure CdS and C_3N_4 . The highest photocatalytic activity was obtained over the 10% C_3N_4/CdS nanocomposites with about 98% RhB decomposed within 120 min. The enhanced photocatalytic property can be possibly attributed to the efficient

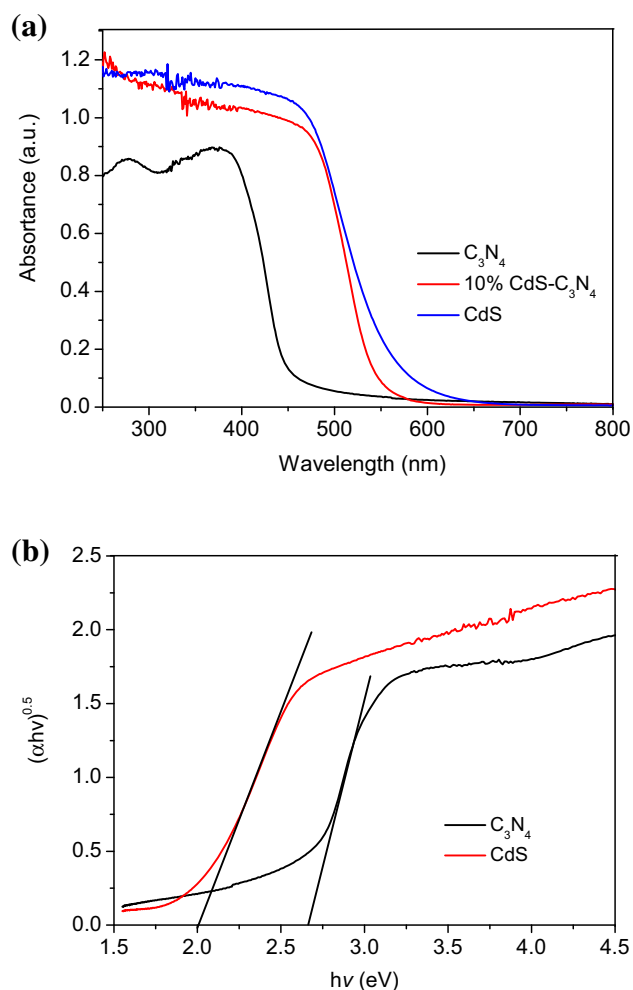


Figure 3. (a) The UV-Vis diffuse reflectance spectra of CdS, C_3N_4 and 10% C_3N_4/CdS . (b) The band gap energies of pure CdS and C_3N_4 .

heterojunction interface in C_3N_4/CdS nanocomposites, which can restrain the recombination of photogenerated electrons and holes. At low CdS content the increase of CdS may result in more heterojunction interface in C_3N_4/CdS nanocomposites, which will suppress the recombination of photo-induced electron-hole pairs. However, the photodegradation efficiency may decrease when the CdS content is higher than 10%, which may be due to the reason that the excessive CdS with narrow band-gap could act as the recombination sites of the electron-hole pairs. To determine the photocatalytic activity quantitatively, the reaction kinetics constant k was investigated by fitting the plots of $\ln(C/C_0)$ vs. irradiation time t according to the pseudo-first-order model $\ln(C/C_0) = kt$, as shown in figure 5. Where C and C_0 are the concentrations of RhB at $t = t$ and 0, respectively. The reaction constant k for RhB degradation on pure C_3N_4 , CdS, 5% C_3N_4/CdS , 10% C_3N_4/CdS and 15% C_3N_4/CdS are 0.00557, 0.00754, 0.00918, 0.02364 and 0.01256 min^{-1} , respectively. The results demonstrate that 10% C_3N_4/CdS exhibits the highest

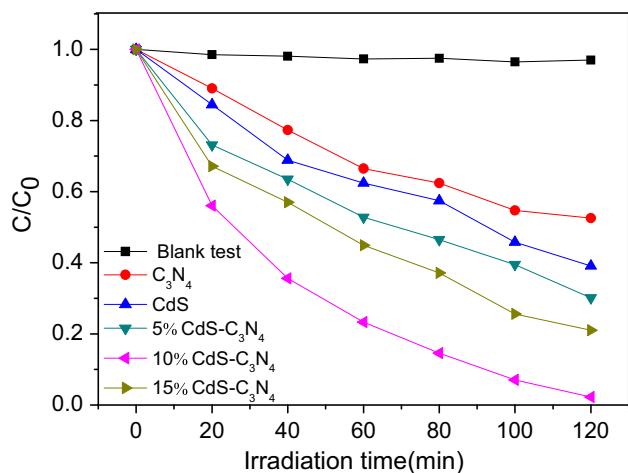


Figure 4. Photocatalytic degradation of RhB over CdS, C_3N_4 and C_3N_4/CdS samples under visible light irradiation.

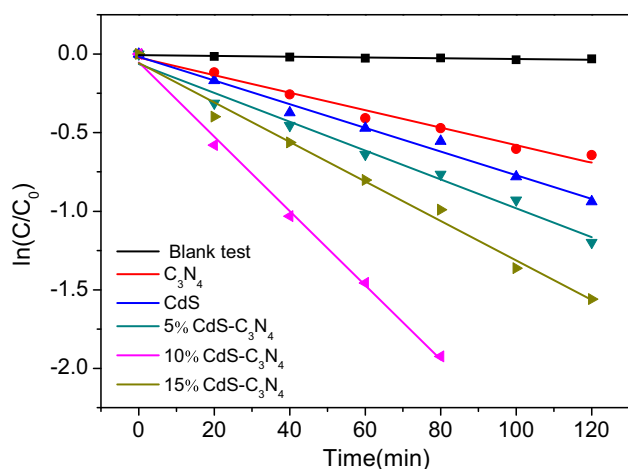


Figure 5. The kinetics for RhB degradation in the presence of as-prepared products under visible light irradiation.

apparent reaction rate constant, indicating greatly enhanced photocatalytic activity on 10% C_3N_4/CdS . The stability of the photocatalysts was also investigated by recycling the 10% C_3N_4/CdS sample that performed the best photocatalytic activity used to degrade RhB. As shown in figure 6, the photocatalytic activity of RhB decomposition on 10% C_3N_4/CdS did not have obvious decrease after three cycles. Thus, the 10% C_3N_4/CdS nanocomposites showed good stability for photocatalytic applications during the photocatalytic reaction.

Photocurrent measures are a useful technique to characterize the separation efficiency of the photo-induced charge carriers in a semiconductor, since the photocurrent mainly results from the transfer of free carriers. Figure 7 shows the photocurrent experiment of the 10% C_3N_4/CdS composites compared with that of pure CdS and C_3N_4 . All the photocurrents descended and ascended periodically with light-off and light-on at an interval of 10 s, which is recyclable and steady

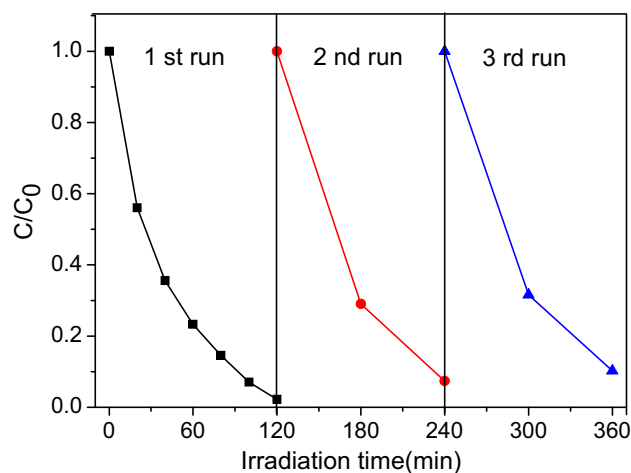


Figure 6. Cycling run in the photocatalytic degradation of RhB.

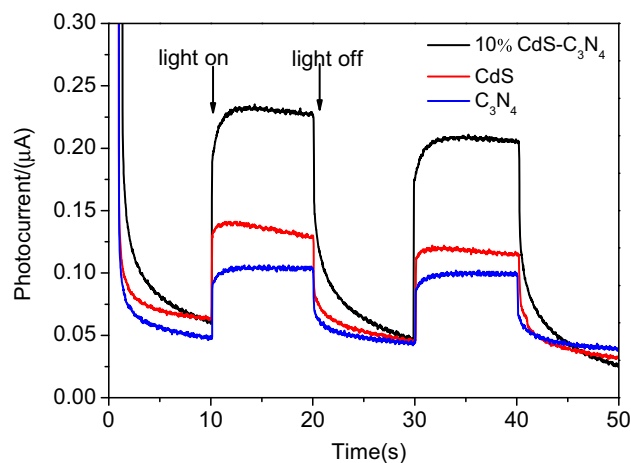


Figure 7. Photocurrent responses of the pure CdS, C_3N_4 and 10% C_3N_4/CdS samples.

during the several on-off irradiation cycles. It can also be seen that 10% C_3N_4/CdS displayed the highest photocurrent than that of CdS and C_3N_4 , and thus had the highest photocatalytic property, which is in accordance with the results from photodegradation experiment.

As is well known, the hydroxyl radicals ($\cdot OH$), photo-induced holes (h^+) and superoxide anion radicals ($\cdot O_2^-$) are three main species for the photo-degradation of RhB. Therefore, trapping experiments of $\cdot OH$, h^+ and $\cdot O_2^-$ were examined in an attempt to elucidate the photocatalytic mechanism in the photodegradation process on the 10% C_3N_4/CdS nanocomposites. Isopropyl alcohol, benzoquinone and KI were used as $\cdot OH$, $\cdot O_2^-$ radicals and h^+ scavengers, respectively. As shown in figure 8, the photodegradation efficiency of RhB hardly changed when isopropyl alcohol was added. On the contrary, the degradation rate of RhB decreased significantly upon addition of benzoquinone and KI. The above results indicate that $O_2^{\cdot -}$ radicals and h^+ were the main

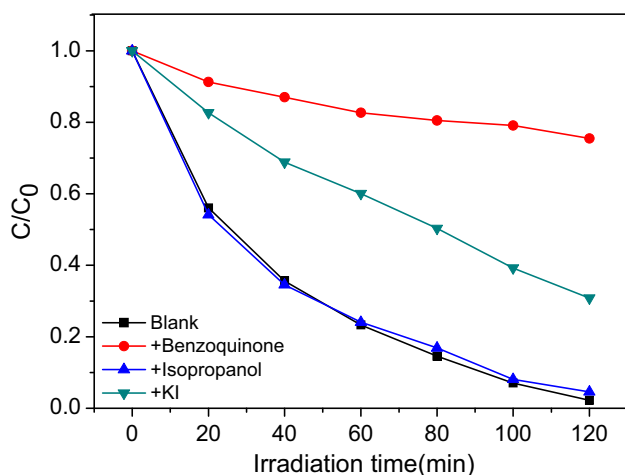


Figure 8. The effects of isopropyl alcohol, benzoquinone and KI on the degradation of RhB with the 10% C_3N_4/CdS samples.

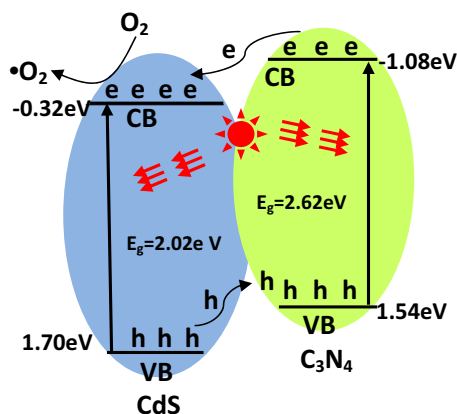


Figure 9. Proposed mechanism for photocatalytic degradation of RhB by the C_3N_4/CdS samples.

active oxidative species for the photodegradation of RhB on the 10% C_3N_4/CdS nanocomposites.

Based on the above-mentioned experimental results and analysis, the mechanism of the enhanced photocatalytic activity of RhB decomposition on the C_3N_4/CdS nanocomposites is presented in figure 9. Under visible light irradiation, both CdS and C_3N_4 in the nanocomposite can be excited to generate photogenerated electron-hole pairs. The photoinduced electrons on the conduction band of C_3N_4 can move quickly to CdS for the conduction band potential of C_3N_4 (-1.08 eV) is more negative than that of CdS (-0.32 eV). In addition, these photogenerated electrons may further react with the adsorbed O_2 molecules on the CdS surface to generate $O_2^{\bullet-}$ radicals, because the valence band potential of C_3N_4 ($+1.54$ eV) is more negative than that of CdS ($+1.70$ eV), the photo-induced holes on the CdS surface can transfer easily to the valence band of C_3N_4 . Therefore, the photo-induced electron-hole pairs are separated efficiently on the nanocomposite interface. This can lead to the C_3N_4/CdS nanocomposites that have

increased photocatalytic activity. At the same time, the holes and $O_2^{\bullet-}$ radicals on the C_3N_4/CdS nanocomposites surface could oxidize the RhB molecules into H_2O , CO_2 and other intermediates.

4. Conclusion

In summary, a g- C_3N_4 hybridized CdS nanoparticles photocatalyst was successfully prepared via a successive calcination and hydrothermal process. Enhanced photocatalytic performance of the C_3N_4/CdS nanocomposites has been observed. The highest photocatalytic activity was obtained over the 10% C_3N_4/CdS nanocomposites with about 98% RhB decomposed within 120 min. The holes and $O_2^{\bullet-}$ radicals generated on the C_3N_4/CdS nanocomposites surface played an important role in the photodegradation of RhB.

References

- [1] Cao Q W, Cui X, Zheng Y F and Song X C 2016 *J. Alloys Compd.* **670** 12
- [2] Yin H, Wang X, Wang L, Nie Q, Zhang Y, Yuan Q *et al* 2016 *J. Alloys Compd.* **657** 44
- [3] Yin H, Wang X, Wang L, Nie Q and Zhao H 2015 *J. Alloys Compd.* **640** 68
- [4] Yin H, Wang X, Wang L, Nie Q, Zhang Y and Wu W 2015 *Mater. Res. Bull.* **72** 176
- [5] Kumar S, Surendar T, Kumar B, Baruah A and Shanker V 2013 *J. Phys. Chem. C* **117** 26135
- [6] Liu W, Wang M, Xu C, Chen S and Fu X 2013 *J. Mol. Catal. A* **368** 9
- [7] He Y, Cai J, Li T, Wu Y, Lin H, Zhao L *et al* 2013 *Chem. Eng. J.* **721** 215
- [8] Wang Y, Bai X, Pan C, Heb J and Zhu Y 2012 *J. Mater. Chem.* **22** 11568
- [9] Fu J, Tian Y, Chang B, Xi F and Dong X 2012 *J. Mater. Chem.* **22** 21159
- [10] Lan Y, Qian X, Zhao C, Zhang Z, Chen X and Li Z 2013 *J. Colloid Interface Sci.* **395** 75
- [11] Shi Y, Li H, Wang L, Shen W and Chen H 2012 *ACS Appl. Mater. Interfaces* **4** 4800
- [12] Li Q, Guo B, Yu J, Ran J, Zhang B and Yan H 2011 *J. Am. Chem. Soc.* **133** 10878
- [13] Khanchandani S, Kundu S, Patra A and Ganguli A K 2012 *J. Phys. Chem. C* **116** 23653
- [14] Zhang L J, Li S, Liu B K, Wang D J and Xie T F 2014 *ACS Catal.* **4** 3724
- [15] Zhang J Y, Wang Y H, Jin J, Zhang J, Lin Z, Huang F *et al* 2013 *ACS Appl. Mater. Interfaces* **5** 10317
- [16] Matsumoto S, Xie E and Izumi F 1999 *Diam. Relat. Mater.* **8** 1175
- [17] Li W T, Zheng Y F, Yin H Y and Song X C 2015 *J. Nanopart. Res.* **17** 271
- [18] Cui X, Huang W Z, Zhou H, Yin H Y, Zheng Y F and Song X C 2015 *Curr. Nanosci.* **11** 360